

Cone Structure and Function in *RPGR*- and *USH2A*-Associated Retinal Degeneration



PAUL S. MICEVYCH, JESSICA WONG, HAO ZHOU, RUIKANG K. WANG, TRAVIS C. PORCO, JOSEPH CARROLL, AUSTIN ROORDA, AND JACQUE L. DUNCAN


- **PURPOSE:** To compare cone structure and function between *RPGR*- and *USH2A*-associated retinal degeneration.
- **DESIGN:** Retrospective, observational, cross-sectional study.
- **METHODS:** This multicenter study included 13 eyes (9 participants) with *RPGR*-related X-linked retinitis pigmentosa (*RPGR*), 15 eyes (10 participants) with *USH2A*-related Usher syndrome type 2 (*USH2*), 16 eyes (9 participants) with *USH2A*-related autosomal recessive retinitis pigmentosa (*ARRP*), and 7 normal eyes (6 participants). Structural measures included cone spacing and density from adaptive optics scanning laser ophthalmoscopy and photoreceptor inner segment (*IS*), outer segment (*OS*), and outer nuclear layer (*ONL*) thickness from optical coherence tomography (*OCT*) images. *OCT* angiography images were used to study choriocapillaris flow deficit percent (*CCFD*). Cone function was assessed by fundus-guided microperimetry. Measures were compared at designated regions using analysis of variance with pairwise comparisons among disease groups, adjusted for disease duration and eccentricity.
- **RESULTS:** *OCT* segmentation revealed shorter *OS* and *IS*, with reduced *ONL* thickness in *RPGR* compared to normal (*OS*: $P < .001$, *IS*: $P = .001$, *ONL*: $P = .005$), *USH2* (*OS*: $P = .01$, *IS*: $P = .03$, *ONL*: $P = .03$), or *ARRP* (*OS*: $P = .001$, *ONL*: $P = .03$). Increased cone spacing was observed in both *RPGR* ($P = .03$) and *USH2* compared with normal ($P = .048$). The mean *CCFD* in *RPGR* was greater than in *USH2* ($P = .02$). Microperimetry demonstrated below-normal regional sensitivity in *RPGR* ($P = .004$), *USH2* ($P = .02$), and *ARRP* ($P = .009$), without significant intergroup differences.

- **CONCLUSIONS:** Outer retinal structure and choriocapillaris perfusion were more abnormal in *RPGR*- than *USH2A*-related retinal degenerations, whereas there were no significant differences in below-normal regional sensitivity between each rod-cone degeneration associated with variants in these 2 genes expressed at the photoreceptor-connecting cilium. (*Am J Ophthalmol* 2023;250: 1–11. © 2023 The Authors. Published by Elsevier Inc. This is an open access article under the CC BY-NC-ND license (<http://creativecommons.org/licenses/by-nc-nd/4.0/>))

RETINITIS PIGMENTOSA (RP) DESCRIBES A DIVERSE group of inherited retinal disorders associated with rod, then cone, dysfunction, and degeneration. RP has a prevalence of approximately 1 in 4000 people worldwide and may be inherited through autosomal dominant, autosomal recessive, X-linked recessive, or mitochondrial patterns.¹ Mutations of the retinitis pigmentosa GTPase regulator (*RPGR*) gene are associated with the majority of X-linked RP and usually start with night blindness beginning in childhood, although some patients with *RPGR*-related retinal degeneration develop cone-rod dystrophy instead of RP.² Mutations in the *USH2A* gene are the most common causes of autosomal recessive RP (*ARRP*) and Usher syndrome type 2 (*USH2*) rod-cone degeneration with congenital hearing loss.³

Despite varied age of onset and rate of degeneration, the products of both *RPGR* and *USH2A* localize to the photoreceptor connecting cilia in both rods and cones, and both play important roles in protein transport between the inner and outer segments.^{4,5} The *RPGR* protein is believed to regulate entry and retention of soluble proteins within photoreceptor cilia.⁴ The *USH2A* protein (usherin) is postulated to interact with the connecting cilium through its large extracellular domain to perform structural and signaling functions.⁵

The relationship between photoreceptor structure and function in retinal degenerations has been studied, yet much remains incompletely understood. Structurally, foveal cone density is lower than normal in both *RPGR*- and *USH2A*-related RP, as measured with adaptive optics scanning laser ophthalmoscope (AOSLO) imaging.^{6,7} In

 Supplemental Material available at [AJO.com](http://ajoc.com).
Accepted for publication January 9, 2023.

From the Department of Ophthalmology, University of California (P.S.M., J.W., T.C.P., J.L.D.), San Francisco, California; Department of Bioengineering, University of Washington (H.Z., R.K.W.), Seattle, Washington; Francis I. Proctor Foundation, Department of Ophthalmology, University of California (T.C.P.), San Francisco, California; Department of Ophthalmology & Visual Sciences, Medical College of Wisconsin Eye Institute (J.C.), Milwaukee, Wisconsin; Herbert Wertheim School of Optometry & Vision Science, University of California Berkeley (A.R.), Berkeley, California, USA

Inquiries to Jacque L. Duncan, Clinical Ophthalmology, Retina Service, University of California, San Francisco, California, USA; e-mail: jacque.duncan@ucsf.edu

© 2023 THE AUTHORS. PUBLISHED BY ELSEVIER INC.

0002-9394/\$36.00

THIS IS AN OPEN ACCESS ARTICLE UNDER THE CC BY-NC-ND LICENSE

<https://doi.org/10.1016/j.ajo.2023.01.006>

([HTTP://CREATIVECOMMONS.ORG/LICENSES/BY-NC-ND/4.0/](http://creativecommons.org/licenses/by-nc-nd/4.0/))

patients with *RPGR*-related X-linked RP (*RPGR*), inner and outer segment lengths on optical coherence tomography (OCT) are shorter than normal even early in disease.^{8,9} Functionally, microperimetry has been used to monitor decreased sensitivity in both *RPGR*-⁷ and *USH2A*-related retinal degeneration.^{10,11} Best-corrected visual acuity, full-field stimulus thresholds, and electroretinogram amplitudes are reduced to a greater degree in *USH2*- compared to *USH2A*-related *ARRP*.^{10,11} Even after accounting for differences in disease duration, visual field sensitivity and total hill of vision measures are reduced in *USH2*- compared with *USH2A*-related *ARRP*.^{10,11}

Although cone structure and function have been shown to decline in RP associated with mutations in both *RPGR* and *USH2A*,^{7,8,10,11} some studies have shown a correlation between cone structure and function in patients with *RPGR*,¹² whereas others have demonstrated more severely reduced cone function for a given cone density in patients with *RPGR*- compared with *RHO*-related RP.⁹ Although *RPGR* and *USH2A* are both expressed at the photoreceptor connecting cilium, few studies have compared measures of cone structure and function between these forms of ciliopathy-related retinal degeneration. Moreover, the widespread use of OCT angiography enables assessment of the outer retinal blood supply by visualizing choriocapillaris flow, but few studies have characterized choriocapillaris flow in *USH2A*-related RP¹³ or compared flow between *RPGR*- and *USH2A*-related retinal degenerations.

As of this writing, there are no approved disease-modifying therapies for *RPGR*- or *USH2A*-related retinal degenerations, but gene-based clinical trials for RP associated with mutations in each are underway. In *RPGR*, an adeno-associated virus gene therapy administered via subretinal injection has shown potential in a dog model,^{14,15} and phase 1 clinical trial results have shown safety.¹⁶ In *USH2A*-related retinal degeneration, RNA antisense oligonucleotide-induced axonal skipping via intravitreal injection has similarly shown promise.¹⁷

With interventions on the horizon, understanding the relationships between degeneration in cone structure and function will be increasingly important. Any dissociation between structure and function in these 2 ciliopathies may signal potential for improvement in function with therapy. In this study, we sought to better understand differences in cone degeneration between *RPGR*- and *USH2A*-associated retinal degeneration (*USH2* and *ARRP*) by comparing cone structure and function through multimodal retinal imaging.

METHODS

• **PARTICIPANTS:** This multicenter, observational, cross-sectional study included participants with *RPGR* recruited from a natural history clinical trial (NCT 04926129), par-

ticipants with *USH2A*-related *ARRP*, participants with *USH2A*-related *USH2*, and normal control participants. Informed consent was obtained for all participants. This research was approved prospectively by the Institutional Review Boards of the University of California, San Francisco, and the Medical College of Wisconsin; was performed in accordance with the Health Insurance Portability and Accountability Act regulations; and followed the tenets of the Declaration of Helsinki.

Participants underwent complete dilated ophthalmologic examination, including measurement of refractive error and best-corrected visual acuity following the Early Treatment of Diabetic Retinopathy Study protocol.¹⁸ Axial length was measured using partial coherence interferometry (IOL Master; Carl Zeiss Meditec), and widefield color and short wavelength autofluorescence fundus photos (California rg; Optos Inc.) were acquired. Genetic testing was performed through the eyeGENE research consortium¹⁹ or next-generation sequencing panel testing through My Retina Tracker, a research database for patients and families with inherited retinal diseases (NCT 02435940).

Inclusion criteria for participants consisted of the clinical and genetic diagnosis of *RPGR*, *USH2*, or *ARRP* and the presence of unambiguous cones at regions of interest (ROIs) in AOSLO images, where information from different imaging modalities was compared. Among the 44 eyes with disease, 39 were imaged at the University of California, San Francisco and 5 were imaged at the Medical College of Wisconsin.

• IMAGING PROTOCOLS AND ANALYSIS:

Spectral domain OCT

Horizontal cross-sectional spectral domain OCT scans (Spectralis; Heidelberg Engineering) extending 15°, 20°, or 30° were acquired on 37 eyes through the fovea, using the manufacturer's automated retinal tracking technology with an average of 100 scans to increase the signal-to-noise ratio. Cross-sectional OCT images were manually segmented to measure outer segment (OS), inner segment (IS), and outer nuclear layer (ONL; including Henle fiber layer) thickness as previously described.^{7,9, 20-22} IS thickness was measured from the external limiting membrane (ELM) to the IS/OS band, OS thickness was measured from the IS/OS band to the OS/RPE band, and ONL thickness was measured from the ELM to the external border of the outer plexiform layer.^{7,9}

OCT layers were segmented throughout the horizontal and vertical scans through the fovea of each eye. The scans were aligned with the AOSLO confocal montages, and the location of each ROI was identified on the superimposed OCT scan. The thickness of each retinal layer at that location was derived from the interpolated segmentation within each eye. In each segmentation, the center of the fovea was marked and aligned with the foveal center identified on AOSLO images based on the location of the foveal pit

on the OCT scans that were precisely aligned using retinal vascular landmarks. The interpolated OCT thickness measurements from each layer in the segmentation data, at the center of the region where the cones were measured, were identified and correlated with all other structural and functional measures at that location. ROIs were not identified at fixed eccentricity from the fovea, but rather areas of identifiable unambiguous cone mosaics on AOSLO. Variable eccentricity was adjusted for in all statistical analyses.

AOSLO images

High-resolution, noninvasive confocal and split-detector images were acquired on 50 eyes with custom AOSLO imaging systems as described in previous work.^{9,23-26} The University of California, San Francisco, system used 840-nm light for imaging and tracking the retina and 910-nm light for wavefront sensing. The light sources were drawn from a supercontinuum light source (SuperK EXTREME; NKT Photonics) using a custom fiber-coupling optical system. A custom Shack Hartman wavefront sensor generated wavefront measurements. A 97-actuator continuous membrane deformable mirror was used for aberration correction (DM97; ALPAO).

Individual AOSLO videos (512 × 496 pixels) covering a 1.2° × 1.2° retinal field of view were acquired at 30 frames per second. The Medical College of Wisconsin system used an 850-nm superluminescent diode as the wavefront sensing source, a near-infrared reflectance imaging source between 775 and 790 nm, and acquired images at 16.6 frames per second with a 1° × 1° or 1.5° × 1.5° field of view.^{27,28} Each video was converted to a high signal-to-noise image after correction for eye movements.^{29,30} Images were assembled into larger montages using custom software designed to align overlapping locations on the horizontal meridian (<https://github.com/BrainardLab/AOAutomontaging>).³¹ AOSLO montages were used to identify regions of interest (ROIs) within each eye, defined as areas with identifiable, unambiguous cone mosaics.

Cone spacing and density at each ROI was computed using custom software (Translational Imaging Innovations, Hickory, NC) as previously described³² using a density recovery profile histogram to identify the mean nearest neighbor distance,³³ and the ratio of number of bound Voronoi cells to the total area of the bound Voronoi cells to define density.^{6,32} Cone spacing was converted to Z score to account for the relationship between cone spacing and eccentricity based on a normal database of 40 normal participants aged 18-82 years (mean 33.6 years, SD 13.7 years).

Swept source OCT angiography

Images extending 6 × 6 mm centered on the fovea were acquired on 46 eyes using a central wavelength of 1060 nm and speed of 100 kHz, with FastTrac motion correction employed to improve image quality. Using previously established methods,^{34,35} the en face OCT angiography image (PLEX Elite 9000; Carl Zeiss Meditec, Inc) was divided

into a grid centered on the fovea and comprised 36 squares, each extending 2° × 2°. The choriocapillaris flow deficit was identified from the OCT angiography image of a 15-μm slab beneath Bruch membrane as pixels with an intensity that is smaller than 1 SD below the mean intensity calculated from a normal database.³⁴ The choriocapillaris flow deficit percentage (CCFD) was then quantified as an area ratio of the segmented flow deficits in the selected region. The CCFD for the grid square corresponding to each ROI in the AOSLO montages was selected for statistical analysis and comparison.

Fundus-guided microperimetry

Fundus-guided microperimetry (macular integrity assessment [MAIA]; CenterVue, Inc.) was acquired under mesopic conditions on 35 eyes. Real-time fundus tracking of retinal images at 25 frames per second were obtained using a scanning laser ophthalmoscope (SLO) and centered around the macula using fundus landmarks, stabilized with eye tracking to compensate for eye movements. Next, to generate a map of MAIA regional sensitivity data points, 1024 × 1024-pixel Goldmann III stimuli (26 arcmin) within a dynamic range of 0-36 dB were projected from an 850-nm superluminescent diode for 200 ms at standard locations separated by 2° across a field ranging from 18° × 18° (Figure 3) to 24° × 24° (Figure 2) field of view of the macula. The field tested varied because some RPGR participants were enrolled in a separate natural history study (NCT 04926129) according to the study protocol used in that trial. Sensitivities at each of the superimposed ROI locations were obtained by interpolating the MAIA data points using the natural neighbor interpolation method³⁶ in MATLAB (MathWorks).

Image overlays

Overlays were created to topographically align fundus photos, OCT, OCT angiography, AOSLO, and microperimetry using Adobe Illustrator (Adobe Systems, Inc) as shown in Figure 1. Images were superimposed manually using retinal vascular landmarks and the optic nerve for guidance. The structural, functional, and perfusion measures were compared at ROIs where unambiguous cone mosaics were identified on AOSLO montages.

- **STATISTICAL ANALYSIS:** Measures of structure (IS thickness, OS thickness, ONL thickness, and cone density), function (regional sensitivity), and perfusion (CCFD) were compared at ROIs between RPGR, USH2, ARRP, and normal eyes. To evaluate relationships between structure and function, the ratio of regional sensitivity to cone density⁹ was also calculated for each group and compared across groups. For all analyses, analysis of variance with pairwise comparisons were clustered by both eye and participant, and adjusted for both disease duration and ROI eccentricity, using linear fixed effects regression analyses. Statistical significance was set at $P < .05$ for all analyses.

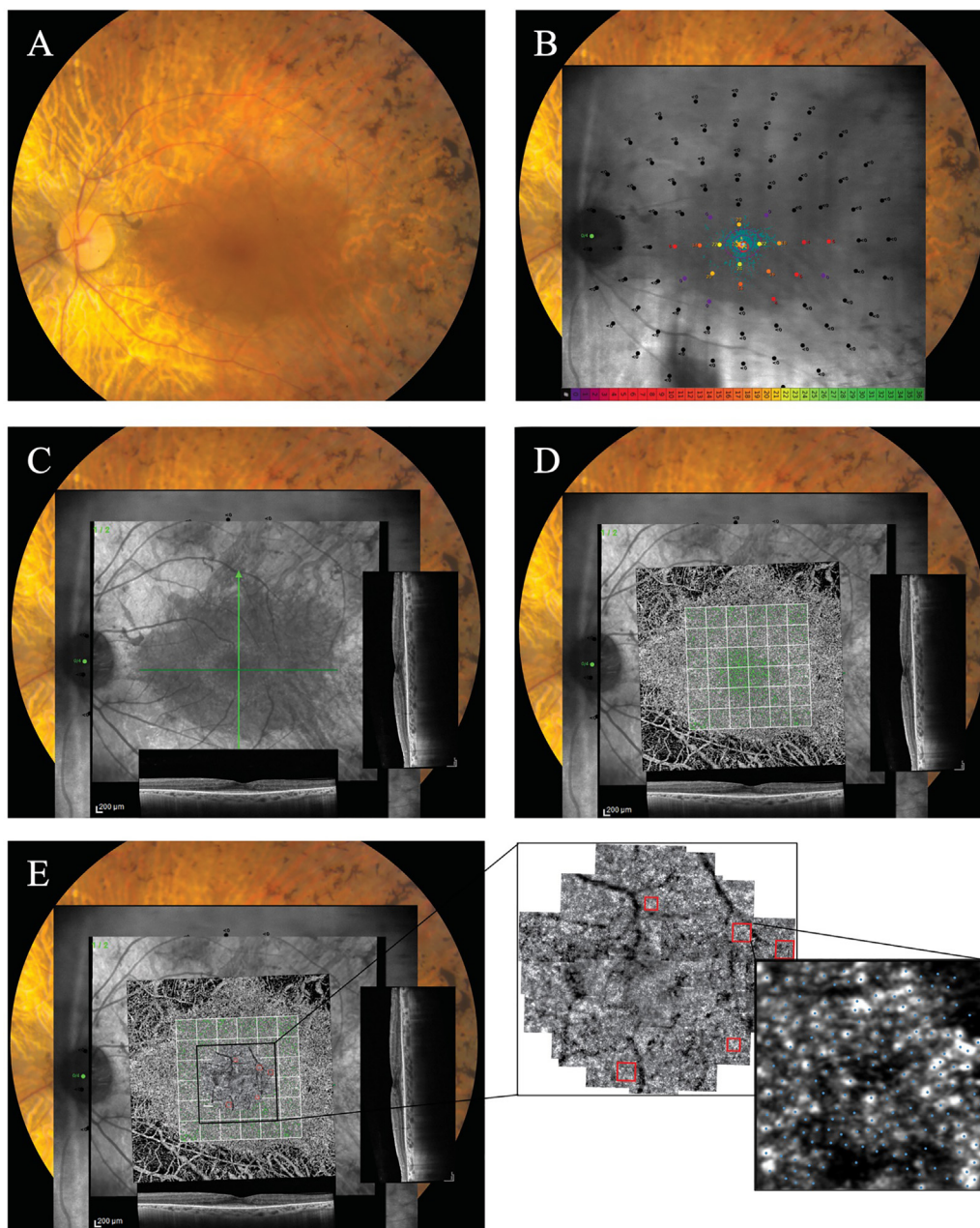


FIGURE 1. Overlay of retinal imaging modalities used to compare structural, functional, and perfusion measures at designated regions of interest for an eye with USH2 (40161, left eye). A. Fundus photograph demonstrating optic disc pallor, vascular attenuation, and midperipheral bone spicule pigmentation. B. Fundus-guided microperimetry sensitivity map superimposed with colored dots representing sensitivity noted on color bar. C. Infrared en face fundus image superimposed with corresponding horizontal and vertical OCT cross sections; green lines indicate scan locations. D. OCT angiography choriocapillaris flow deficit map with $2^\circ \times 2^\circ$ macular grid superimposed, demonstrating areas of flow deficit in green. E. Adaptive optics scanning laser ophthalmoscopy confocal montage aligned using retinal vascular landmarks; individual cones identified (blue dots) within a selected, magnified region of interest (red squares). OCT = optical coherence tomography.

RESULTS

- **PARTICIPANTS:** Participant demographics, clinical characteristics, and mutation analyses are reported in [Table 1](#).

The study included 13 eyes (9 participants) with RPGR, 15 eyes (10 participants) with USH2, 16 eyes (9 participants) with ARRP, and 7 normal eyes (6 participants). Mean age \pm SD was 22.1 ± 8.6 years among RPGR participants, 33.6 ± 16.8 years among USH2 participants, 46.3 ± 6.5 years

TABLE 1. Participant Demographics, Genetic Analyses, and Clinical Characteristics

	ID	Eye	Sex	Age, y	Genetic Mutation	Symptom Duration, y	BCVA (decimal)
RPGR	40015	OD	M	25	c.2426_2427del	13	0.50
	40049	OS	M	26	c.1245+2T>C	22	0.50
	40064	OD	M	23	c.1243_1244delAG	8	0.80
		OS				8	1.25
	40080	OS	M	35	c.28+5G>A	25	1.25
	40159	OD	M	27	c.2442_2445del	1	0.80
	40191	OD	M	28	c.2426_2427del, p.Glu809GlyfsX25	10	1.00
		OS				10	1.00
	40214	OD	M	12	Ex5-114/+46, c.356del, p.Leu119TrpfsX14m (hemizygous)	8.5	0.50
		OS				9	0.50
	40215	OS	M	9	c.2168_2171delGAAA, p.Arg723Thrfs*91	9	0.40
	40222	OD	M	14	c.2630del, p.Glu877Glyfs*212 (hemizygous)	3	0.63
		OS			3	0.50	
USH2	DW_0111	OD	F	29	c.5877_delT; p.Ser1961Gln fs *6, partial del exons 22-27	29	0.67
	KS_0588	OD	M	34	c.8682-9A>G splice variant, partial del exons 22-24	unknown	0.80
	KS_10084	OD	F	28	c.9842G>T; p.Cys3281Phe,c.3584G>T; p.Cys1195Phec.15017C>T; p.Thr5006Met	unknown	1.00
	JC_10158	OS	F	36	c.2299delG; p.Glu767Ser fs *21, c.5836C>T; p.Arg1946Stop	unknown	0.63
	40097	OD	F	34	c.2299delG, p.Glu767SerfsX21 (homozygous)	22	0.63
		OS				22	0.63
	40157	OD	F	19	c.3187_3188del, p.Gln1063Sfs*15 and c.(5298+1_5299-1)_(5572+1_5573-1)del exon 27	19	1.25
		OS				19	1.25
	40161	OS	M	66	TAT>TGT, p.Tyr380Cys and 4bp insertion of CAGC starting in codon 306	38	0.63
	40204	OD	M	15	c.1055C>T, p.Thr3521Ile and c.4108G>C, p.Val1370Leu	13	1.25
OS				13		1.25	
40207	OD	F	58	c.10388-2A>G, c.8655_(8681+1_8682-1)del (partial exon 43 deletion)	48	0.80	

(continued on next page)

TABLE 1. (continued)

ID	Eye	Sex	Age, y	Genetic Mutation	Symptom Duration, y	BCVA (decimal)	
	OS				48	0.80	
40208	OD	M	17	c.9424G>T, p.Gly3142* (pathogenic) and c.10465G>A, p.Ala3489Thr, VUS; in cis	1	1.25	
	OS				1	1.25	
ARRP	DH_10161	OS	F	49	c.10073G>A; p.Cys3358Tyr, c.8016G>A; p.Leu2672Leu	unknown	1.25
	40039	OD	M	48	c.2276G>T, p.Cys759Phe and c.2296T>C, p.Cys766Arg	10	1.25
	OS				10	1.25	
40043	OD	F	38	c.2296 G>T, p.Cys759Phe and c.del exons 12-16, c.(1971+1_1972-1)_(3316+1_3317-1)	18	0.80	
	OS				18	0.80	
40082	OD	M	44	c.8522G>A, p.W2841X and c.11266G>A, p.G3756S	20	0.50	
	OS				20	0.50	
40110	OD	F	47	c.11156G>A, p.Arg3719His and c.8659dup, p.Tyr2887Leufs*2	21	0.80	
40151	OD	F	58	c.11864G>A, p.Trp3955* and c.6835G>C, p.Asp2279His	4	0.50	
	OS				4	0.50	
40162	OD	M	48	c.(6325+1_6326-1)_(6657+1_6658-1) del exons 33-34 and c.12575G>A, p.Arg4192His	6	0.80	
	OS				6	0.80	
40163	OD	M	49	c.2276G>T, p.Cys759Phe and c.1036A>C, p.N346H	3	1.00	
	OS				3	1.25	
40180	OD	M	36	c.2299del, p.Glu767Serfs*21 and c.2276G>T, p.Cys759Phe	3	1.25	
	OS				3	0.80	
Normal	10003	OS	M	52			1.25
	40104	OS	M	26			1.25
	40154	OS	F	23			1.00
	40171	OS	F	81			1.00
	40179	OD	F	31			1.00
	40201	OD	M	66			0.80
	OS						0.80

ARRP = autosomal recessive retinitis pigmentosa, BCVA = best-corrected visual acuity.

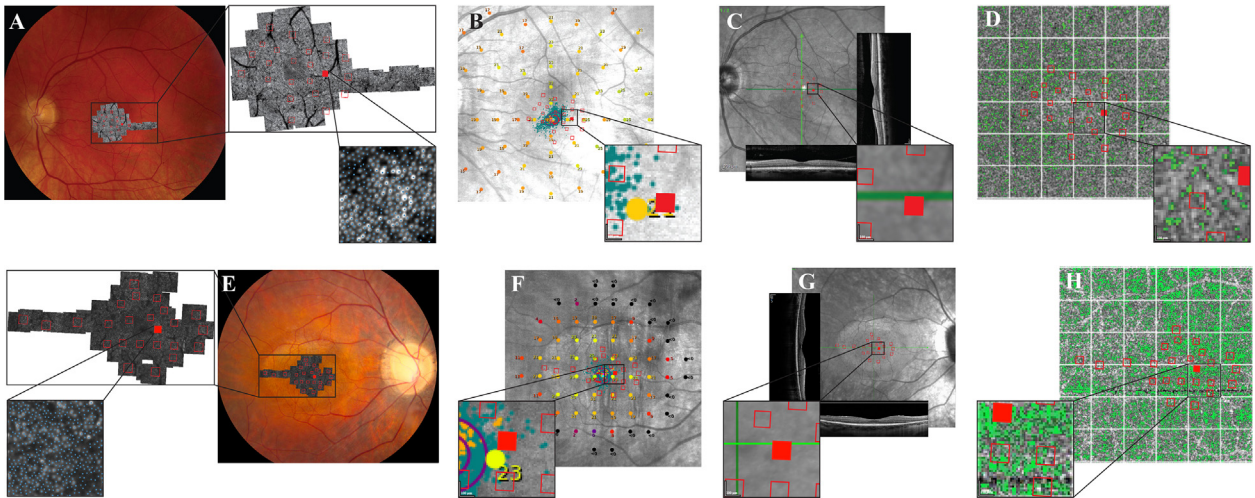


FIGURE 2. Representation of multimodal imaging methods compared at a single designated ROI (solid red box) in eyes with ARRP (upper row; participant 40163 OS) and RPGR (lower row; participant 40191 OD). Fundus photograph with superimposed adaptive optics scanning laser ophthalmoscopy confocal montage with designated ROI magnified to demonstrate cone density methods in (A) ARRP (cone density 2833.16 cones/degree²) and (E) RPGR (cone density 3110.52 cones/degree²). Fundus-guided microperimetry map with magnified 2° by 2° square to demonstrate region sensitivities in (B) ARRP (regional sensitivity 21.76 dB) and (F) RPGR (regional sensitivity 23.75 dB). OCT en face image superimposed with corresponding horizontal and vertical cross sections and green lines to indicate scan locations, magnified to demonstrate location for thickness measurements surrounding designated ROI in (C) ARRP (OS 42.81 μm, IS 29.68 μm, ONL 81.91 μm) and (G) RPGR (OS 22.42 μm, IS 27.81 μm, ONL 95.68 μm). OCT angiography CCFD map with 2° x 2° grid demonstrating areas of flow deficit in green and magnified to demonstrate results for designated ROI in (D) ARRP (CCFD 8.95%) and (H) RPGR (CCFD 29.29%). Note region eccentricity from the fovea of 2.20° in ARRP and 1.40° in RPGR. ARRP = autosomal recessive retinitis pigmentosa, CCFD = choriocapillaris flow deficit, IS = inner segment, OCT = optical coherence tomography, ONL = outer nuclear layer, OS = outer segment, ROI = region of interest.

among ARRP participants, and 46.5 ± 23.7 years among normal participants. Mean symptom duration \pm SD was 9.9 ± 6.9 years in RPGR eyes, 22.8 ± 15.7 years in USH2 eyes, and 9.9 ± 7.3 years in ARRP eyes. All of the RPGR participants were male, whereas 60% of USH2, 44.4% of ARRP, and 50% of normal participants were female. Mean best-corrected visual acuity \pm SD was 0.74 ± 0.3 among RPGR eyes, 0.88 ± 0.3 among ARRP eyes, 0.9 ± 0.35 among USH2 eyes, and 1.01 ± 0.18 among normal eyes.

- **STRUCTURAL MEASURES:** Representative methods and results for each structural and functional measure at a designated ROI are demonstrated in Figure 2. Boxplot comparisons of outcome measures, statistically adjusted for region eccentricity and disease duration, are shown in Figure 3. Median and mean \pm SD for OS thickness (Figure 3 A) were 22.8 and 21.2 ± 10.7 μm in RPGR eyes, 39.0 and 38.4 ± 10.3 μm in USH2 eyes, and 41.6 and 41.7 ± 6.1 μm in ARRP eyes, compared with 38.8 and 38.8 ± 4.5 μm in normal eyes. Mean OS thickness was lower in RPGR ($P < .001$) and USH2 eyes ($P = .037$) compared with normal eyes. Mean OS thickness was lower in RPGR than USH2 ($P = .015$) and ARRP eyes ($P = .0014$).

Median and mean \pm SD for IS thickness (Figure 3, B) were 29.8 and 27.9 ± 7.9 μm in RPGR eyes, 36.2 and 36.0 ± 4.0 μm in USH2 eyes, and 31.8 and 32.5 ± 3.2 μm in

ARRP eyes, compared with 33.9 and 34.2 ± 3.0 μm in normal eyes. Mean IS thickness was lower in RPGR than normal ($P = .0011$) and USH2 eyes ($P = .029$). Median and mean \pm SD for ONL thickness (Figure 3, C) were 100.0 and 100.6 ± 18.7 μm in RPGR eyes, 125.2 and 125.7 ± 13.9 μm in USH2 eyes, and 118.3 and 120.3 ± 13.1 μm in ARRP eyes, compared with 118.3 and 116.6 ± 9.2 μm in normal eyes. Mean ONL thickness was lower in RPGR than normal ($P = .0054$), USH2 ($P = .025$), and ARRP eyes ($P = .027$).

Median and mean \pm SD for cone spacing Z score (Figure 3, D) were 2.0 and 2.6 ± 3.2 in RPGR eyes, 1.1 and 2.0 ± 2.7 in USH2 eyes, and 1.0 and 1.3 ± 1.8 in ARRP eyes, compared with 0.4 and 0.5 ± 1.2 in normal eyes. Mean cone spacing Z score was significantly greater in both RPGR ($P = .025$) and USH2 eyes ($P = .048$) compared with normal eyes. Median and mean \pm SD for cone density (Figure 3, E) were 1664.3 and 1864.9 ± 832.4 cones/degree² in RPGR eyes, 1689.1 and 1958.4 ± 912.1 cones/degree² in USH2 eyes, and 2056.1 and 2271.5 ± 889.4 cones/degree² in ARRP eyes, compared with 1863.3 and 2189.1 ± 1044.3 cones/degree² in normal eyes. Mean cone density was reduced in both RPGR ($P = .01$) and USH2 eyes ($P = .012$) compared with normal eyes. No significant differences were found in cone spacing Z score ($P = .24$) or cone density ($P = .36$) between disease groups.

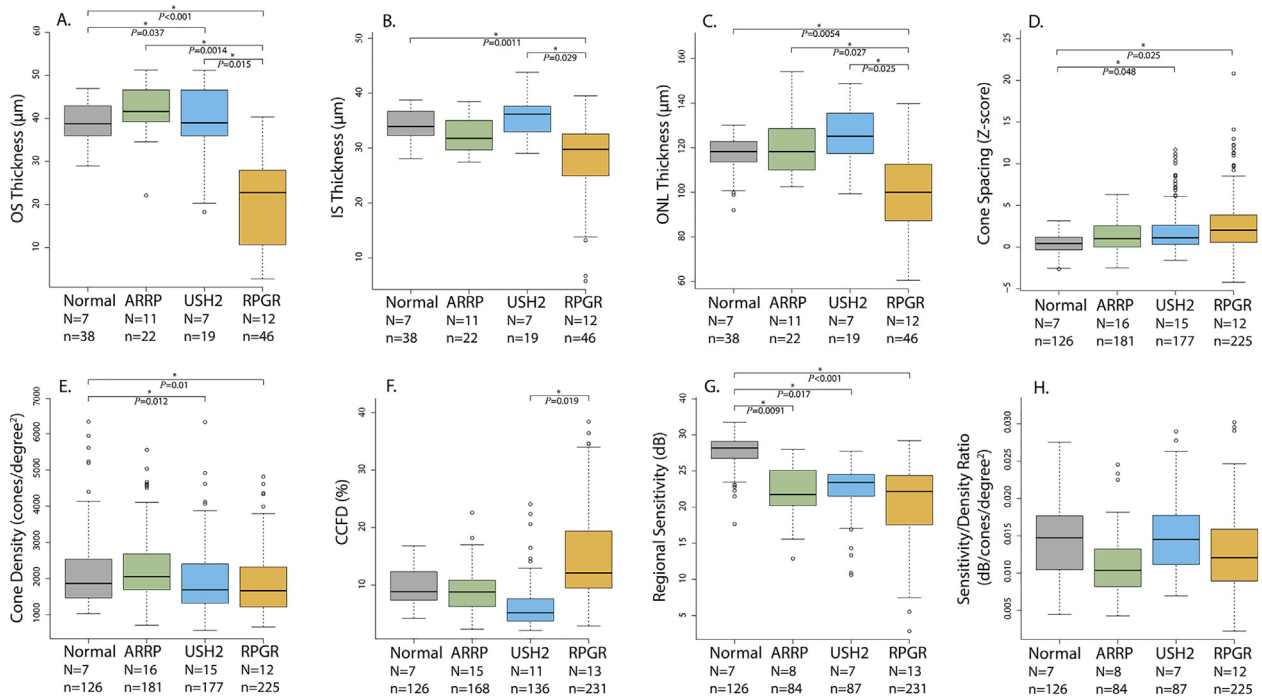


FIGURE 3. Boxplots represent comparisons between structural and functional markers in RPGR, USH2, ARRP, and normal eyes, adjusted for disease duration and region eccentricity. Comparisons in (A-C) outer retinal layer thickness demonstrate thin OS, IS, and ONL thickness in RPGR. Comparisons in (D) cone spacing Z score and (E) cone density demonstrate cone loss in RPGR and USH2. Comparisons in (F) mean CCFD show greater flow deficit in RPGR than USH2. Comparisons in (G) mean regional sensitivity demonstrate reduction from normal across all groups, whereas (H) sensitivity per cone (sensitivity to cone density ratio) remains similar to normal in each group. Asterisks represent statistical significance ($P < .05$). ARRP = autosomal recessive retinitis pigmentosa, CCFD = choriocapillaris flow deficit percent, IS = inner segment, N = number of eyes, n = number of regions of interest, ONL = outer nuclear layer, OS = outer segment.

Median and mean \pm SD for CCFD (Figure 3, F) were 12.1% and $15.1 \pm 8.4\%$ in RPGR eyes, 5.2% and $6.4 \pm 3.8\%$ in USH2 eyes, and 8.8% and $8.8 \pm 3.5\%$ in ARRP eyes, compared to 8.9 and $9.6 \pm 3.1\%$ in normal eyes. There were no significant differences in CCFD between disease groups and normal eyes (RPGR-normal: $P = .16$; USH2-normal $P = .45$; RP-normal $P = .89$). Within disease groups, mean CCFD was greater in RPGR than USH2 ($P = .019$).

• **FUNCTIONAL MEASURES:** Median and mean \pm SD for regional sensitivity (Figure 3, G) were 22.2 and 21.0 ± 4.9 dB in RPGR eyes, 23.4 and 22.6 ± 3.2 dB in USH2 eyes, and 21.7 and 22.3 ± 3.1 dB in ARRP eyes, compared with 28.2 and 27.7 ± 2.2 dB in normal eyes. Compared with normal eyes, mean regional sensitivity was reduced in eyes with RPGR ($P < .001$), USH2 ($P = .017$), and ARRP ($P = .0091$). No significant differences were found in regional sensitivity between disease groups ($P = .31$). Median and mean \pm SD for regional sensitivity to cone density ratio (Figure 3, H) were 0.012 and 0.013 ± 0.005 dB/cones/degree² in RPGR eyes, 0.014 and 0.015 ± 0.005 dB/cones/degree² in USH2 eyes, and 0.010 and 0.011 ± 0.004 dB/cones/degree² in ARRP eyes, compared with

0.015 and 0.015 ± 0.005 dB/cones/degree² in normal eyes. There were no significant differences between disease groups and normal eyes (RPGR-normal $P = .79$; USH2-normal $P = .13$; ARRP-normal $P = .47$), nor between disease groups ($P = .28$).

DISCUSSION

The relationship between cone structure and function was characterized in this study comparing RPGR- and USH2A-related retinal degenerations, each arising from gene products expressed at the photoreceptor connecting cilium and resulting in rod-cone degeneration. Significant differences in outer retinal layer thickness and CCFD without differences in regional sensitivity reveal relative alterations in cone structure, but not function, between RPGR- and USH2A-related retinal degenerations. Among USH2A-related retinal degenerations, USH2 and ARRP exhibited similar levels of cone structural, functional, and vascular alteration. These results reflect a similar impact from variants of their shared pathogenic gene, USH2A.

The participants with RPGR demonstrated more severe disease than *USH2A*-related retinal degeneration in several key cone structural measures. Outer retinal layer thickness, in particular OS thickness, was significantly reduced in RPGR compared with each of the 3 comparison groups (Figure 3, A). These results suggest that OS shortening, a finding also observed in prior work,⁹ is a key feature of RPGR degeneration. OS thickness therefore may be an important structural efficacy outcome measure in retinal gene therapy trials for RPGR and may account for the reduced sensitivity observed in patients with RPGR-related retinal degeneration. RPGR eyes also exhibited a greater degree of choriocapillaris abnormality than *USH2A*-related retinal degeneration, specifically USH2. Greater CCFD, suggesting a reduced choriocapillaris perfusion, was found in RPGR than USH2 (Figure 3, F).

Participants with RPGR- and *USH2A*-related retinal degenerations each exhibited abnormal macular function. Regional sensitivity was significantly reduced compared with normal in all disease groups, with no significant differences found between groups in RPGR, USH2, and ARRP (Figure 3, G), despite shorter OS, IS, and ONL layer thickness in the RPGR patients (Figure 3, A-C). Accounting for disease duration, decreased cone function may be a shared feature among these ciliopathies.

The findings in this study unveil possible discrepancies between structure and function in these retinal degenerations. The differences in outer retinal layer thickness, but not regional sensitivity, between RPGR- and *USH2A*-related retinal degenerations may represent one such disconnect. Prior work has suggested discrepancies in structure and function in RPGR in comparison with other forms of RP using a sensitivity to cone density ratio.⁹ We found no significant differences between groups in the regional sensitivity to cone density ratio. We propose that this discrepancy from prior work⁹ may be best explained by the greater spectrum of disease severity within the current study of a larger number of patients and eyes.

Eyes with RPGR-related RP in the current study had shorter duration of disease and greater OS thickness than in the prior article, and the results of the current work suggest the prior finding of reduced sensitivity to cone density likely resulted from shorter OS per cone in the RPGR patients in that work. Phototransduction occurs in the OS, and prior studies have correlated visual function with ONL and OS thickness in patients with RP.²⁰ We reported reduced sensitivity per cone in the prior work, in which mean OS thickness was lower and duration of disease was greater in patients with RPGR-related RP than in the current study. In the present study, we observed decreased density of cones overall in RPGR, with preserved function per cone, as compared to *USH2A*-related degenerations.

This relative preservation of function in the setting of severe structural abnormalities in RPGR stands in contrast to the greater preservation of structure in the setting of abnormal cone function in *USH2A*-related retinal de-

generations. This may indicate that cone function is relatively preserved even in RPGR eyes with greater structural abnormality, and that clinical measures of cone function may be less sensitive indicators of disease progression than structural measures. Similar redundancy of visual function has been reported in other studies using visual acuity^{37,38} and microperimetry⁷ in other patients with rod-cone degeneration.

This study carries several important strengths and limitations. This is the first study to compare structure and function of RPGR- and *USH2A*-related retinal degenerations. In doing so, this study demonstrates several key quantifiable similarities and differences among retinal degenerations associated with mutations in genes expressed at the photoreceptor connecting cilia. RPGR carries an earlier age of onset than USH2 or ARRP, and patients in the study with RPGR were notably younger than the other groups.

To account for this, and its impact on disease duration specifically, we adjusted all statistical analyses for disease duration based on the patient's report of first symptom onset. We also considered further correlating visual acuity with structural outcome measures for ROIs within 0.5° of the fovea. However, these were too few for meaningful statistical comparison, particularly in normal eyes, in which foveal cones are not readily visualized.

Other limitations of this study include the small numbers of participants in each group, in keeping with low prevalence of disease. It should also be noted that among the eyes from Medical College of Wisconsin, imaging was limited to AOSLO and 4 eyes were of unknown disease duration (KS_0588, KS_10084, JC_10158 and DH_10161; Table 1). Moreover, all imaging was acquired at a single point in time for each eye in this cross-sectional study, so we are unable to comment on disease progression of the structural and functional outcome measures in this study.

Lastly, we note the inherent limitations of existing imaging methods. In particular, MAIA fundus-guided microperimetry does not carry the precision of AOSLO in targeting function of specific cones. As such, we cannot claim with certainty that RPGR, USH2, and ARRP demonstrate the same functional abnormalities, but rather that these degenerations demonstrate nonsignificant differences in regional sensitivity using our methods. Importantly, we chose to use MAIA fundus-guided microperimetry as it is one of the most widely used metrics for extrafoveal macular function.

In summary, compared with *USH2A*-related retinal degeneration, eyes with RPGR demonstrated a greater reduction in outer retinal layer thickness (most prominently OS thickness) and choriocapillaris perfusion (reflected by greater CCFD), whereas regional sensitivity was reduced among all disease groups. Comparing disease groups, RPGR demonstrated relative preservation of function in the setting of more severe structural degeneration, suggesting that reduced cone function results from loss of cones rather than dysfunction of remaining cones in eyes with RPGR- and

Funding/Support: This research was supported, in part, by the [Foundation Fighting Blindness](#) (Project Award 0617-0708), UCSF Vision Core NIH/NEI P30 EY002162, NIH/NEI Bioengineering Research Partnership R01EY023591, R01EY017607 and by an unrestricted grant from Research to Prevent Blindness. Certain patients were also enrolled in a natural history study sponsored by Biogen/NightstarX Therapeutics (NCT04926129).

Financial Disclosures: J.C. receives financial support from AGTC, MeiraGTx, OptoVue, has personal financial interest in Translational Imaging Innovations, and a patent USPTO 9,427,147. R.K.W. receives financial support and consultancy fees from and has a patent with Carl Zeiss Meditec.

A.R. has patents (USPTO 7,118,216, USPTO 6,890,076) with the University of Rochester and University of Houston, and personal financial interests in C. Light Technologies.

J.L.D. receives consultancy fees from AGTC, California Institute for Regenerative Medicine, ConeSight, DTx Therapeutics, Editas Medicine, EyeVensys, Foundation Fighting Blindness, Gyroscope Therapeutics, Helios, Nacuity, ProQR Therapeutics, PYC Therapeutics, SparingVision, Spark Therapeutics, and Vedere Bio II, and has a nonremunerative relation with Foundation Fighting Blindness, Neurotech USA, Inc. (I, spouse), and RxSight, Inc.

All authors attest that they meet the current ICMJE criteria for authorship.

REFERENCES

1. Verbakel SK, van Huet RAC, Boon CJF, et al. Non-syndromic retinitis pigmentosa. *Prog Retin Eye Res.* 2018;66:157–186.
2. De Silva SR, Arno G, Robson AG, et al. The X-linked retinopathies: physiological insights, pathogenic mechanisms, phenotypic features and novel therapies. *Prog Retin Eye Res.* 2020;100898.
3. Fahim A. Retinitis pigmentosa: recent advances and future directions in diagnosis and management. *Curr Opin Pediatr.* 2018;30(6):725–733.
4. Rao KN, Li L, Anand M, et al. Ablation of retinal ciliopathy protein RPGR results in altered photoreceptor ciliary composition. *Sci Rep.* 2015;5:11137.
5. Liu X, Bulgakov OV, Darrow KN, et al. Usherin is required for maintenance of retinal photoreceptors and normal development of cochlear hair cells. *Proc Natl Acad Sci U S A.* 2007;104(11):4413–4418.
6. Sun LW, Johnson RD, Langlo CS, et al. Assessing photoreceptor structure in retinitis pigmentosa and Usher syndrome. *Invest Ophthalmol Vis Sci.* 2016;57(6):2428–2442.
7. Foote KG, De la Huerta I, Gustafson K, et al. Cone spacing correlates with retinal thickness and microperimetry in patients with inherited retinal degenerations. *Invest Ophthalmol Vis Sci.* 2019;60(4):1234–1243.
8. Menghini M, Jolly JK, Nanda A, et al. Early cone photoreceptor outer segment length shortening in RPGR X-linked retinitis pigmentosa. *Int J Ophthalmol.* 2021;244(4):281–290.
9. Foote KG, Wong JJ, Boehm AE, et al. Comparing cone structure and function in RHO- and RPGR-associated retinitis pigmentosa. *Invest Ophthalmol Vis Sci.* 2020;61(4):42.
10. Birch DG, Cheng P, Duncan JL, et al. The RUSH2A study: best-corrected visual acuity, full-field electroretinography amplitudes, and full-field stimulus thresholds at baseline. *Transl Vis Sci Technol.* 2020;9(11):9.
11. Duncan JL, Liang W, Maguire MG, et al. Baseline visual field findings in the RUSH2A study: associated factors and correlation with other measures of disease severity. *Am J Ophthalmol.* 2020;219:87–100.
12. Bellingrath JS, Ochakovski GA, Seitz IP, et al. High symmetry of visual acuity and visual fields in RPGR-linked retinitis pigmentosa. *Invest Ophthalmol Vis Sci.* 2017;58(11):4457–4466.
13. Hagag AM, Mitsios A, Gill JS, et al. Characterisation of microvascular abnormalities using OCT angiography in patients with biallelic variants in USH2A and MYO7A. *Br J Ophthalmol.* 2020;104(4):480–486.
14. Dufour VL, Cideciyan AV, Ye GJ, et al. Toxicity and efficacy evaluation of an adeno-associated virus vector expressing codon-optimized RPGR delivered by subretinal injection in a canine model of X-linked retinitis pigmentosa. *Hum Gene Ther.* 2020;31(3-4):253–267.
15. Song C, Dufour VL, Cideciyan AV, et al. Dose range finding studies with 2 RPGR transgenes in a canine model of X-linked retinitis pigmentosa treated with subretinal gene therapy. *Hum Gene Ther.* 2020;31(13-14):743–755.
16. Cehajic-Kapetanovic J, Xue K, Martinez-Fernandez de la Camara C, et al. Initial results from a first-in-human gene therapy trial on X-linked retinitis pigmentosa caused by mutations in RPGR. *Nat Med.* 2020;26(3):354–359.
17. Dulla K, Slijkerman R, van Diepen HC, et al. Anti-sense oligonucleotide-based treatment of retinitis pigmentosa caused by USH2A exon 13 mutations. *Mol Ther.* 2021;29(8):2441–2455.
18. Ferris FL, Kassoff A, Bresnick GH, et al. New visual acuity charts for clinical research. *Am J Ophthalmol.* 1982;94(1):91–96.
19. Sullivan LS, Bowne SJ, Reeves MJ, et al. Prevalence of mutations in eyeGENE probands with a diagnosis of autosomal dominant retinitis pigmentosa. *Invest Ophthalmol Vis Sci.* 2013;54(9):6255–6261.
20. Birch DG, Wen Y, Locke K, et al. Rod sensitivity, cone sensitivity, and photoreceptor layer thickness in retinal degenerative diseases. *Invest Ophthalmol Vis Sci.* 2011;52(10):7141–7147.
21. Hood DC, Cho J, Raza AS, et al. Reliability of a computer-aided manual procedure for segmenting optical coherence tomography scans. *Optom Vis Sci.* 2011;88(1):113–123.
22. Hood DC, Lin CE, Lazow MA, et al. Thickness of receptor and post-receptor retinal layers in patients with retinitis pigmentosa measured with frequency-domain optical coherence tomography. *Invest Ophthalmol Vis Sci.* 2009;50(5):2328–2336.
23. Scoles D, Sulai YN, Langlo CS, et al. In vivo imaging of human cone photoreceptor inner segments. *Invest Ophthalmol Vis Sci.* 2014;55(7):4244–4251.
24. Duncan JL, Zhang Y, Gandhi J, et al. High-resolution imaging with adaptive optics in patients with inherited retinal degeneration. *Invest Ophthalmol Vis Sci.* 2007;48(7):3283–3291.
25. Merino D, Dainty C, Bradu A, et al. Adaptive optics enhanced simultaneous en-face optical coherence tomog-

- raphy and scanning laser ophthalmoscopy. *Opt Express*. 2006;14(8):3345–3353.
26. Merino D, Duncan JL, Tiruveedhula P, et al. Observation of cone and rod photoreceptors in normal subjects and patients using a new generation adaptive optics scanning laser ophthalmoscope. *Biomed Opt Express*. 2011;2(8):2189–2201.
 27. Drew S, Sulai YN, Langlo CS, et al. In vivo imaging of human cone photoreceptor inner segments. *Invest Ophthalmol Vis Sci*. 2014;55(7):4244–4251.
 28. Litts KM, Georgiou M, Langlo CS, et al. Interocular symmetry of foveal cone topography in congenital achromatopsia. *Curr Eye Res*. 2020;45(10):1257–1264.
 29. Stevenson SB, Roorda A, Kumar G. Eye tracking with the adaptive optics scanning laser ophthalmoscope. *Proceedings of the 2010 Symposium on Eye-Tracking Research and Applications - ETRA ACM*; 2010:195–198.
 30. Stevenson SB, Roorda A. Correcting for miniature eye movements in high resolution scanning laser ophthalmoscopy. In: Manns F, Soderberg P, Ho A, eds. *Ophthalmic Technologies XI SPIE*; 2005:145–151.
 31. Chen M, Cooper RF, Han GK, et al. Multi-modal automatic montaging of adaptive optics retinal images. *Biomed Opt Express*. 2016;7(12):4899–4918.
 32. Cooper RF, Wilk MA, Tarima S, Carroll J. Evaluating descriptive metrics of the human cone mosaic. *Invest Ophthalmol Vis Sci*. 2016;57(7):2992–3001.
 33. Rodieck RW. The density recovery profile: a method for the analysis of points in the plane applicable to retinal studies. *Vis Neurosci*. 1991;6(2):95–111.
 34. Zhang Q, Zheng F, Motulsky EH, et al. A novel strategy for quantifying choriocapillaris flow voids using swept-source OCT angiography. *Invest Ophthalmol Vis Sci*. 2018;59(1):203–211.
 35. Nattagh K, Zhou H, Rinella N, et al. OCT angiography to predict geographic atrophy progression using choriocapillaris flow void as a biomarker. *Transl Vis Sci Technol*. 2020;9(7):6–6.
 36. Amidror I. Scattered data interpolation methods for electronic imaging systems: a survey. *J Electron Imaging*. 2002;11(2):157–176.
 37. Ratnam K, Carroll J, Porco TC, et al. Relationship between foveal cone structure and clinical measures of visual function in patients with inherited retinal degenerations. *Invest Ophthalmol Vis Sci*. 2013;54(8):5836–5847.
 38. Bensinger E, Rinella N, Saud A, et al. Loss of foveal cone structure precedes loss of visual acuity in patients with rod-cone degeneration. *Invest Ophthalmol Vis Sci*. 2019;60(8):3187–3196.